Supplementary Materials for "Powering a Microprocessor by Photosynthesis"

This PDF file includes:

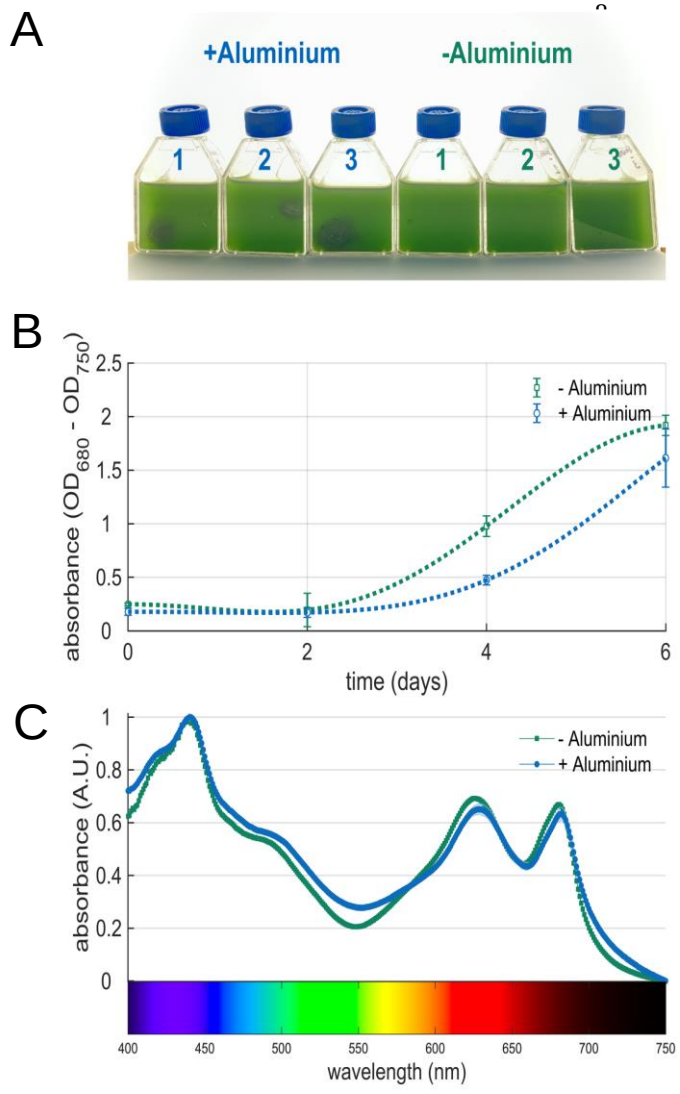

Fig. S1. Growth of *Synechocystis* in the presence of aluminium wool. **A**) Flasks of *Synechocystis* with or without aluminium (three replicates, six days after inoculation). **B**) Growth curves for *Synechocystis* with or without aluminium. **C**) Normalised absorption spectra for cell suspension of *Synechocystis* with or without aluminium.

Fig. S2. Aluminium wool used in this study. **A,B**) Photographs of the filaments of aluminium at two different magnifications. The filaments are up to 300 mm long and have a diameter varying from 100 µm to 300 µm.

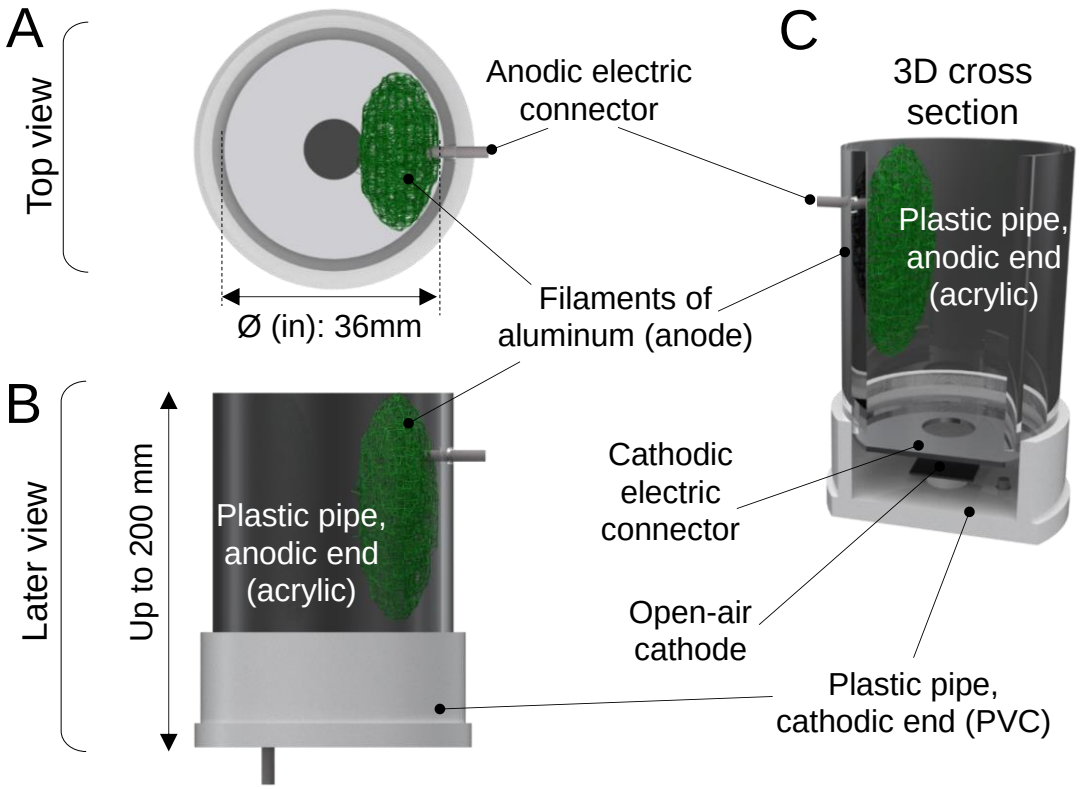

Fig. S3. Structure of the prototype Al-BPV system. **A,B**) Diagram of the key components and dimensions forming the prototype Al-BPV system, top and lateral view respectively. **C**) 3D cross section of the of prototype Al-BPV system displaying the key components.

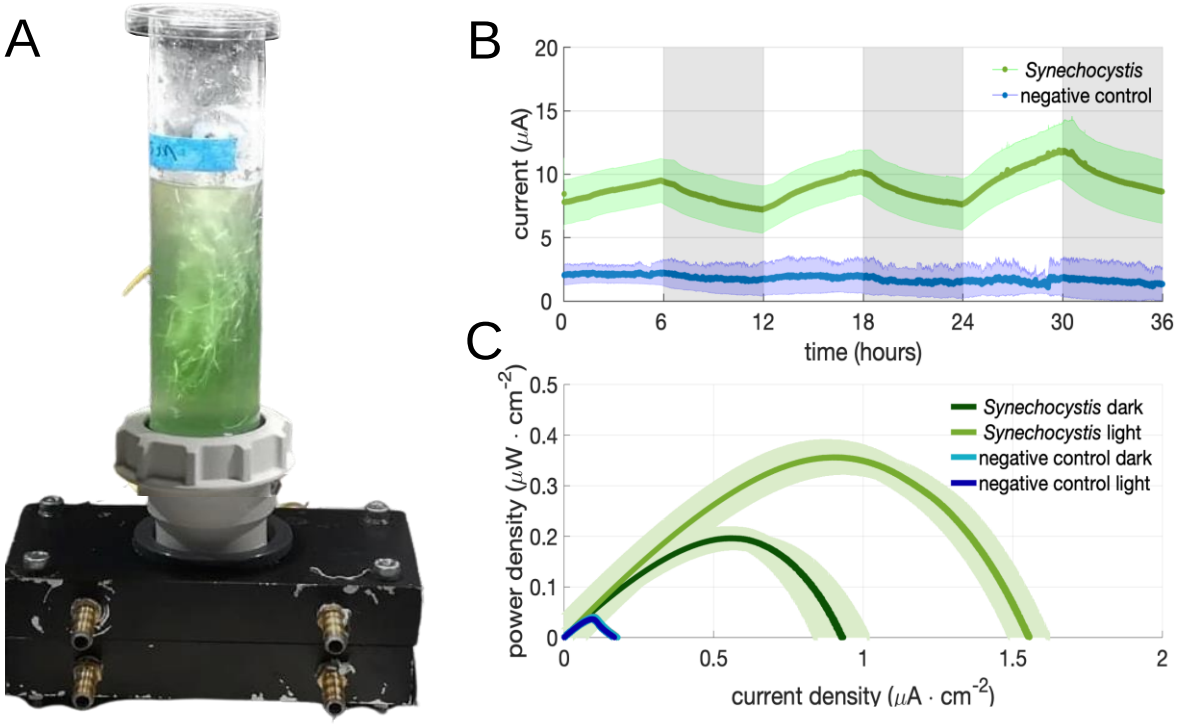

Fig. S4. Performance of the prototype Al-BPV system. **A)** Photo of the prototype Al-BPV system used for laboratory testing and operated with *Synechocystis*. **B**) Current generated by aluminium anodes colonised by *Synechocystis* (green trace) or for abiotic negative control (blue trace) in the prototype Al-BPV. White and dark panels represent periods of light and dark respectively. Current was measured using a MultiEmStat Potentiostat in chronoamperometry mode with bias potential of 0V. **C)** Power curves for prototype Al-BPV systems under dark (dark green trace) and light (light green trace) respectively (n=3). The green shadow represents the standard deviation of the mean (n=3). Blue traces indicate the abiotic negative controls under dark (light blue trace) and light (dark blue trace) respectively (n=3). Current and power intensity were normalised by the total illuminated surface of the BPV (10.2 cm^2) to calculate the reported current and power densities. Illumination was provided by warm-white LED placed at the top. The measured peak power densities per unit area for *Synechocystis* in dark and light, respectively, were 0.197 ± 0.023 μW cm^{-2} and 0.361 ± 0.034 μW cm^{-2}. The measured peak power densities per unit area for the negative control in dark and light, respectively, were 0.041 ± 0.001 μW cm^{-2} and 0.037 ± 0.003 μW cm^{-2}. Using the above peak power densities, a two-sample student t-test (ttest2 in Matlab R2021) was performed to assess the statistical significance of the differences in peak power densities between anodes with *Synechocystis* and autoclaved anodes (negative control). The test comparing *Synechocystis* and negative control anodes in the light rejected the null hypothesis that there was no difference (H = 0) and returned a p-value (significant at the 5% level) of 0.0051. The test comparing *Synechocystis* and negative control anodes in the dark rejected the null hypothesis (H = 0) and returned a p-value (significant at the 5% level) of 0.0169.

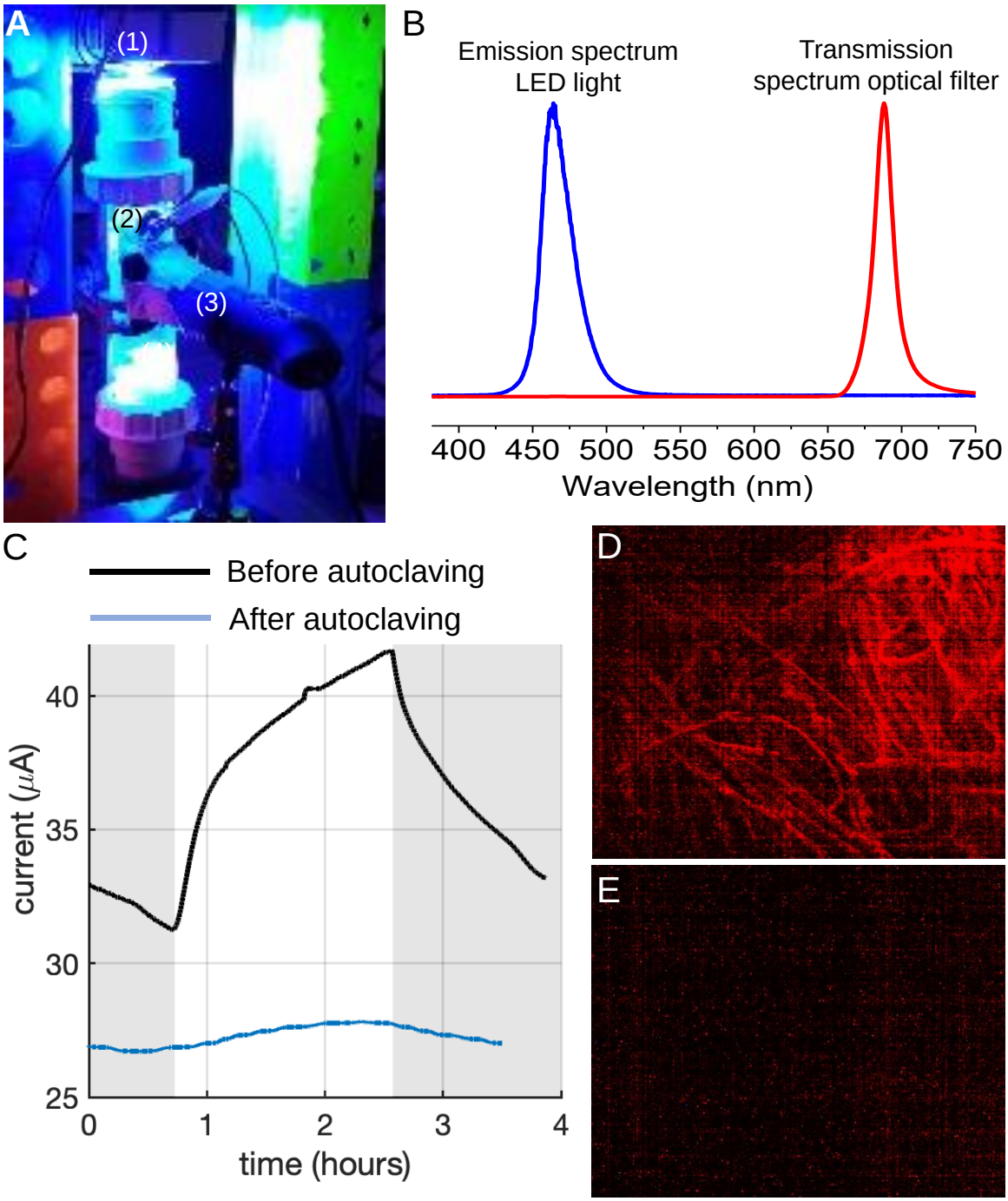

Fig. S5. Autofluorescence and current output measured from a prototype Al-BPV system 12 months old **A**) Experimental set-up used to observe autofluorescence. LED light source (1); Al-BPV system (2); optical filter (3); digital camera (4). **B**) Emission spectrum of the LED light (λ=475nm, blue line) and transmission spectrum (λ=688nm, red line) of the optical filter used. **C**) Current output generated by an Al-BPV system before (black) and after autoclaving (blue). The grey and white backgrounds represent periods of dark and light respectively. **D**) Autofluorescence emitted by an aluminium anode taken with an optical filter in front of the digital microscope. **E**) Autofluorescence emitted by an autoclaved aluminium anode taken with an optical filter in front of the digital microscope.

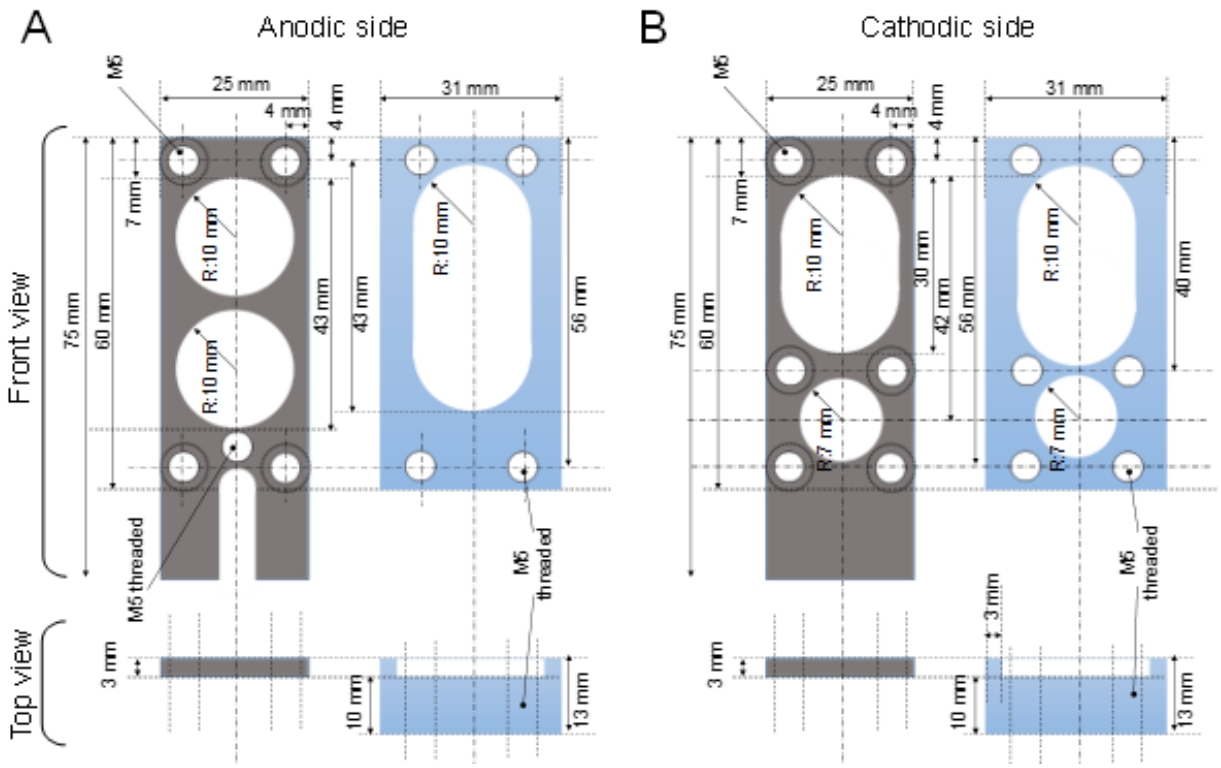

Fig. S6. Diagram of the main components of the compact Al-BPV system used to power the CPU. **A,B**) anodic and cathodic side respectively. The grey and the light blue shades denote stainless-steel and acrylic respectively. The screws holding the components together are not shown in this diagram.

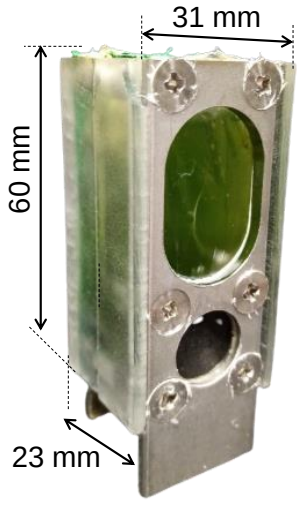

Compact Al-BPV

Width*: 31 x 23 mm
Hight*: 60 mm

Anode: Aluminum filament (0.7 g)
Cathode: Carbon paper-Pt (active area Ø 7 mm)

Body: acrylic block and PTFE film
Electric connectors: stainless-steel metal plates

*dimension of the external system

Fig. S7. Compact Al-BPV system used to power the ultra-low-power processor: dimensions and materials. The body of the Al-BPV was made using acrylic, polytetrafluoroethylene (PTFE) and stainless-steel (S/S) plates. The aluminium anode is fastened to the metal plate using 4 mm stainless-steel screws and washers.

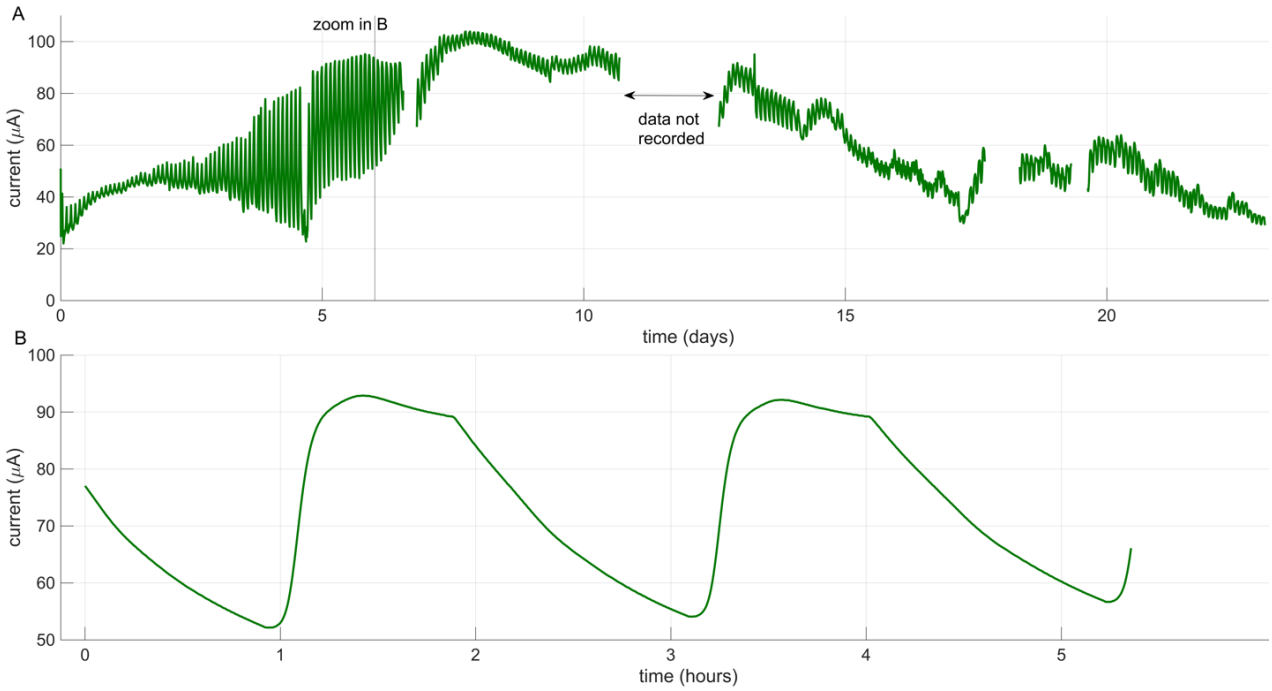

Fig. S8. The compact Al-BPV (**Fig.1C,D** and **Fig.S6,7**) was first tested in a controlled laboratory environment (20-22 °C and white-warm LED light at ~500 μE m^{-2} s^{-1}). The peak power (4.2 μW cm^{-2}) and max current (17.2 μA cm^{-2}) per unit area of the compact Al-BPV determined under laboratory conditions (**Fig.1E**) were comparable to values obtained with other BPV systems. Chronoamperometry of the compact Al-BPV system in a laboratory-controlled environment. (Data recording was lost from day 11 to day 13.) **A)** Current intensity as a function of time during ca. 23 days**. B)** A zoomed-in inset of data in A plotted with hourly resolutions. The LED that illuminated the BPV was programmed to emit light-dark cycles with a period of 2 hours.

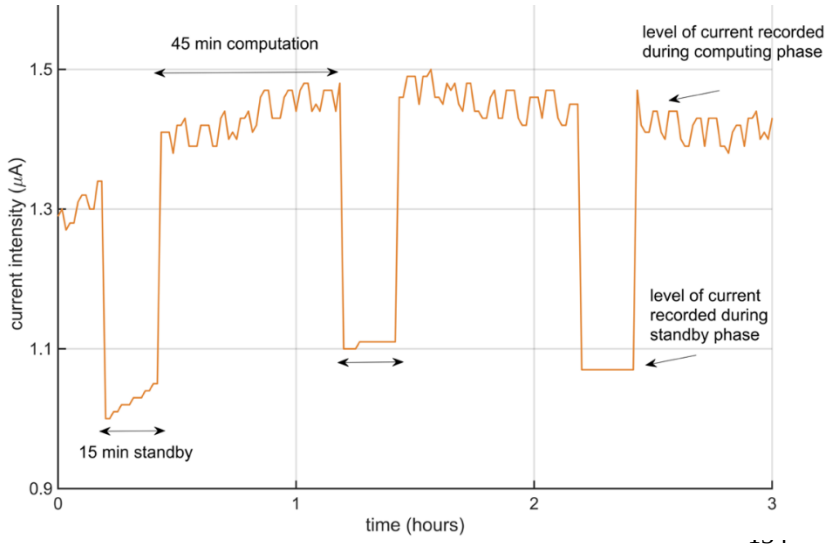

Fig. S9. Example of current recording during the operation of the Cortex-M0+ processor. Variation of the current drawn from the compact Al-BPV system during the CPU cycle of alternating operation (45 minutes in computing mode followed by 15 minutes in standby).

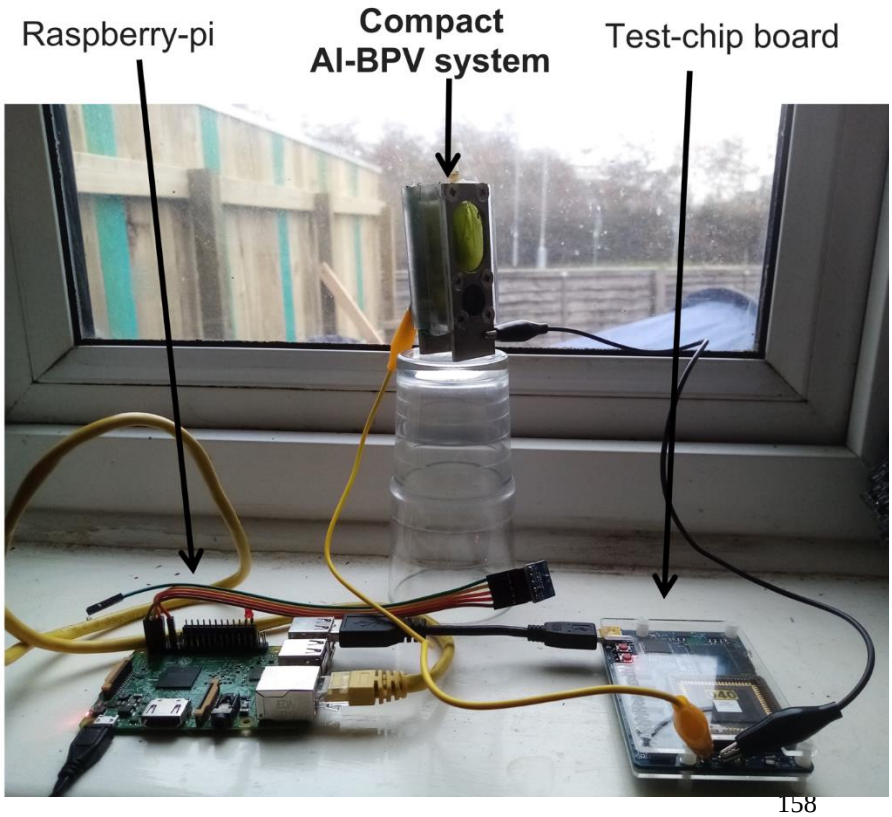

Fig. S10. Domestic environment where the experimental tests were conducted. The compact Al-BPV was placed at the window sill in a living room of a domestic property. The location is in Cambridge (UK), latitude: 52.23 / 52°14'0"N; longitude: 0.1329 / 0°7'58"E.

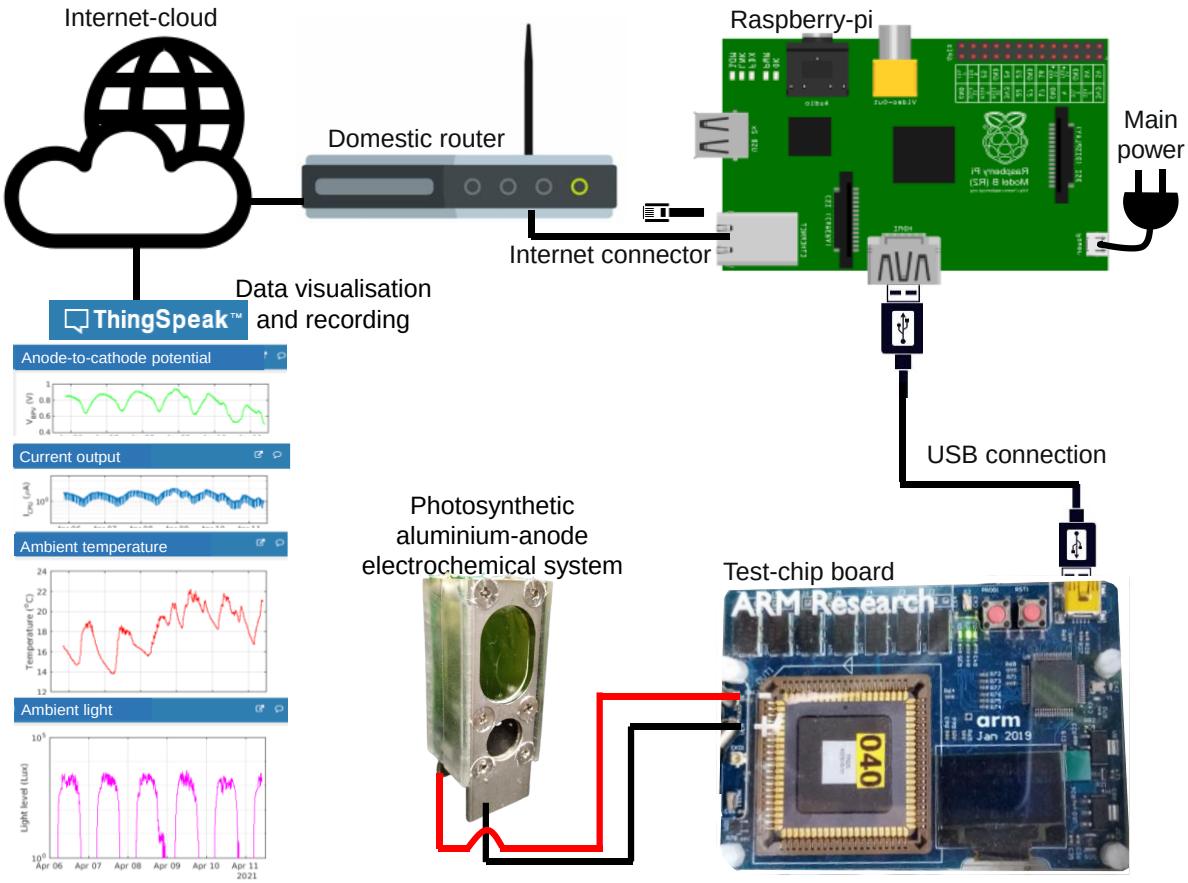

Fig. S11. Compact Al-BPV system powering the processor: Data recording and visualisation. The photosynthetic aluminium-anode electrochemical system powered the Cortex-M0+ processor. The photosynthetic aluminium-anode electrochemical system powers only the Cortex-M0+ processor in the test chip, which consumes a minimum of 0.3 µW (@0.3V). The test-chip board verifies the operation of the processor and measures the potential and intensity of the electrical output of the photosynthetic aluminium-anode electrochemical system. Data are transferred to the Internet-cloud via a Raspberry-pi/router. The rest of the test-chip other than the Cortex-M0+ processor, all other electronic components in the test-chip board, Raspberry-pi and router are powered by the mains power. The ThingSpeak™ platform is used to record and visualise the data (https://thingspeak.com/channels/1033008).

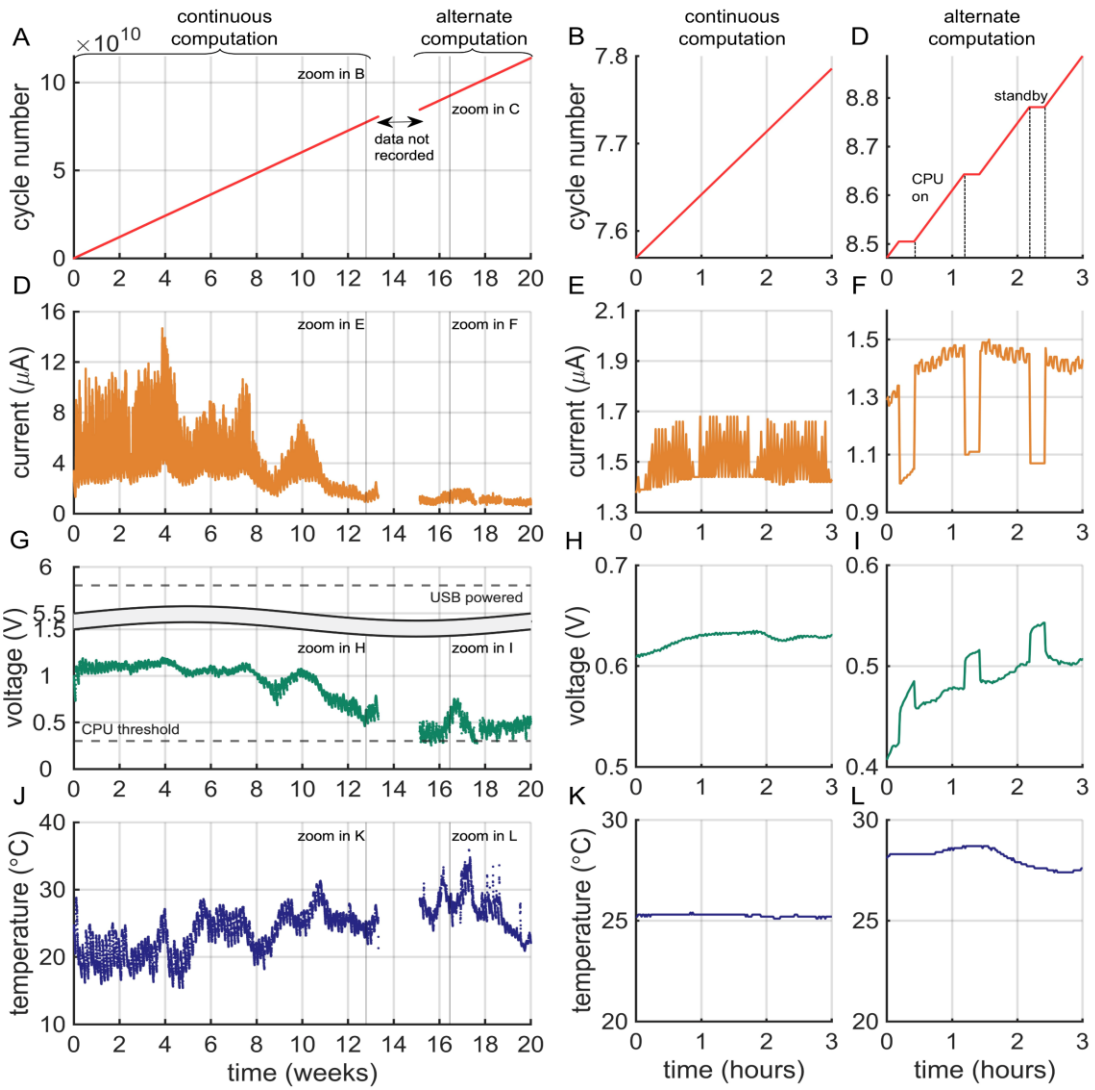

Fig. S12. Powering the Arm Cortex-M0+ processor by the compact Al-BPV system in a domestic environment. The experiment included a first phase (week 0 to week 13) of continuous computation followed by a second phase (week 15 to week 20) during which the CPU alternated in cycles from 45 minutes of computation to 15 minutes of standby. The data presented in the left column (**A,D,G** and **J**) show the entire experimental run. The data presented in the centre column (**B,E,H** and **K**) show three hours of recording taken from an arbitrary point (in continuous computation mode) of the left column. The data presented in the right column (**C,F,I** and **L**) show three hours of recording taken from an arbitrary point of the centre column (in alternate computation mode). **A-C**) Cumulative number of cycles of computation events performed by the CPU. **D-F**) Current generated by the BPV device. **G-I**) Potential difference between the anode and cathode of the BPV device. The dotted line indicates the threshold of potential below which the CPU will stop working. The section above the line break in the y axis indicates the voltage range (5.5-6 V) that would be recorded if the BPV failed to power the CPU (the CPU would then be USB powered). **J-L**) environmental temperature measured by a probe integrated into the test-chip.

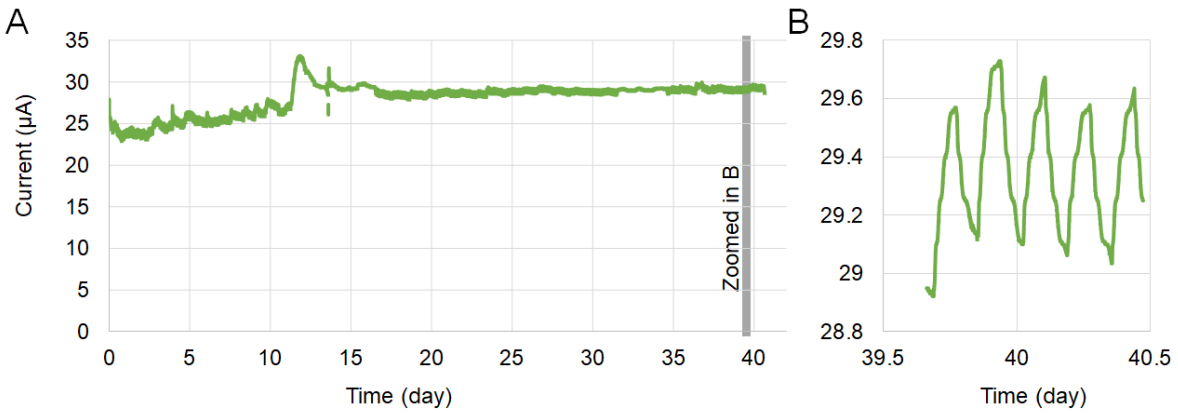

Fig. S13. Current output generated under constant cycles of light and dark by an Al-BPV system that had been operating for more than two years. The light and dark cycle was arbitrarily fixed at 2h:2h **A**) Circa 40 days of continuous recording. **B**) Several hours of recording taken from an arbitrary point (depicted by the grey-shaded regions) in panel **A**.

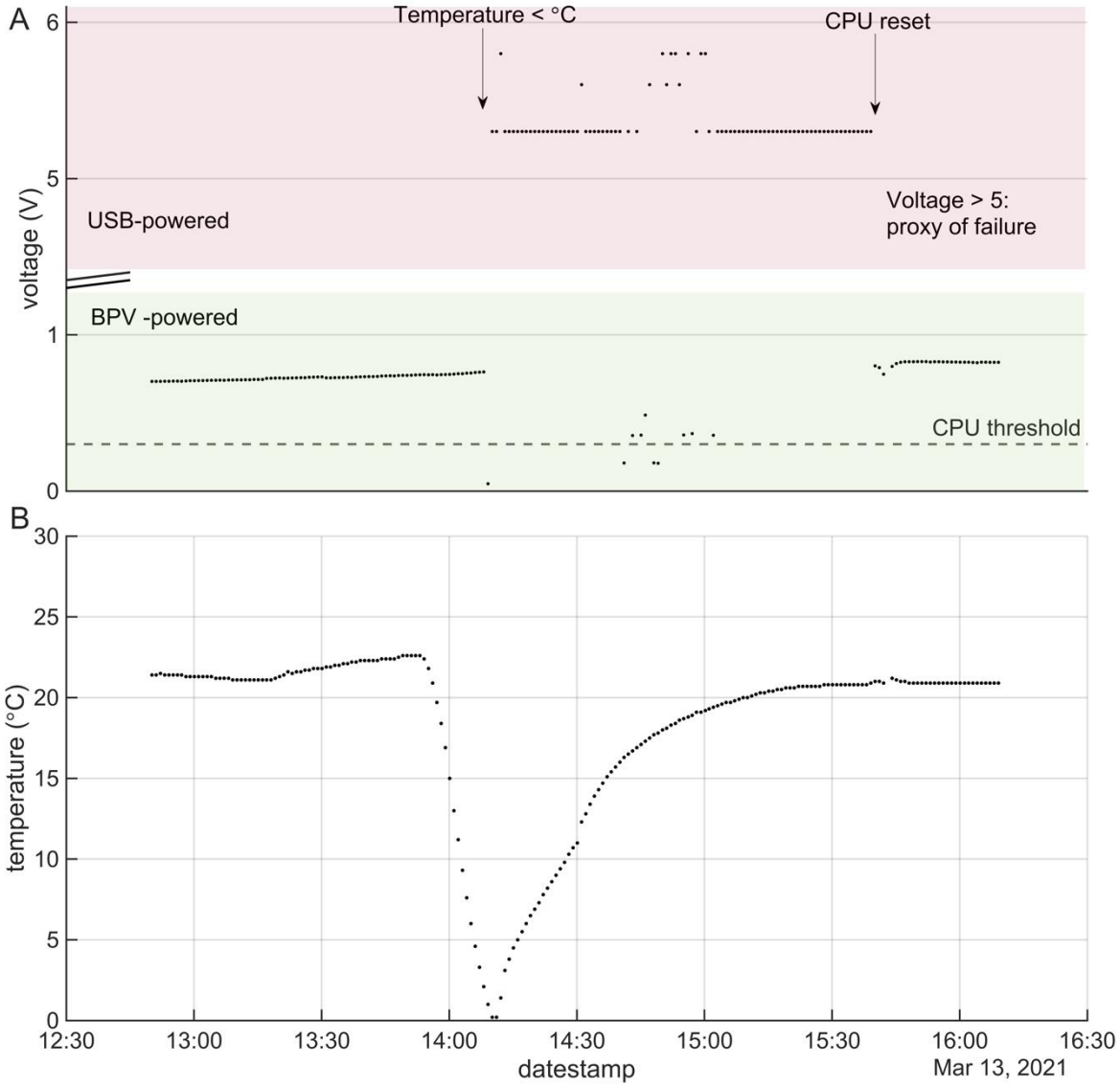

Fig. S14. Change in voltage (**A**) and temperature (**B**) when the compact Al-BPV fails to power the processor. Those data are zoomed from **figure 2G** and **2M** respectively. The pink panel indicates where the processor is powered from an external supply, and the green indicates where it is powered by the Al-BPV. The failure was deliberately induced by lowering the ambient temperature (**B**) below 5 C° with an ice-pack. In this instance, the software controlling the operation of the CPU triggered to switch the power of the processor from the Al-BPV to another electricity supply via a USB which is indicated by recording a voltage >5V.

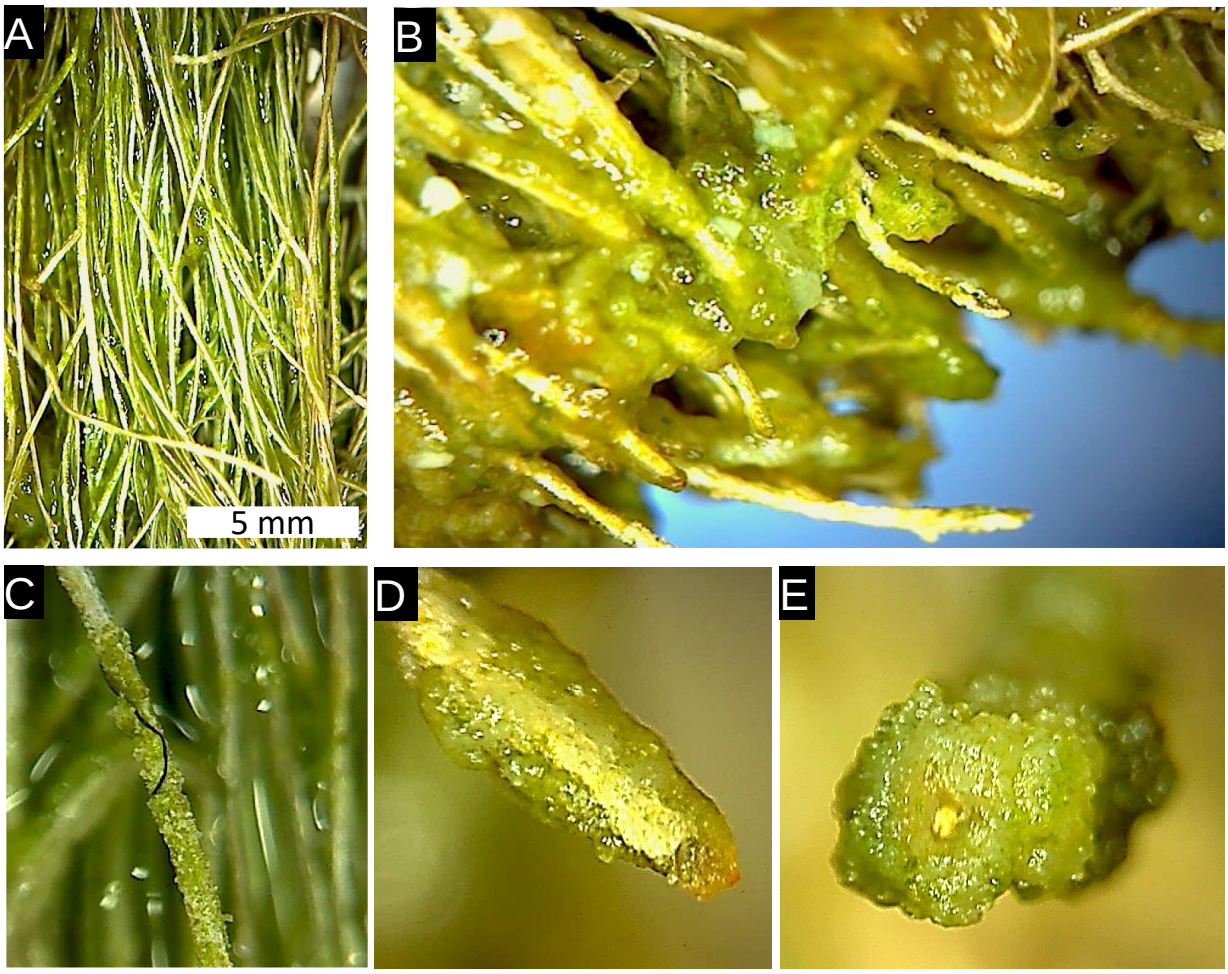

Fig. S15. Filaments from an aluminium anode taken from a mature Al-BPV system several months old. **A-E**) Photograph of the filaments of aluminium anode and matrix (aluminium hydroxide and extracellular components) taken with a stereo microscope at various magnifications and orientations. The filaments have dimeter ranging from 0.2 to 0.4 mm.

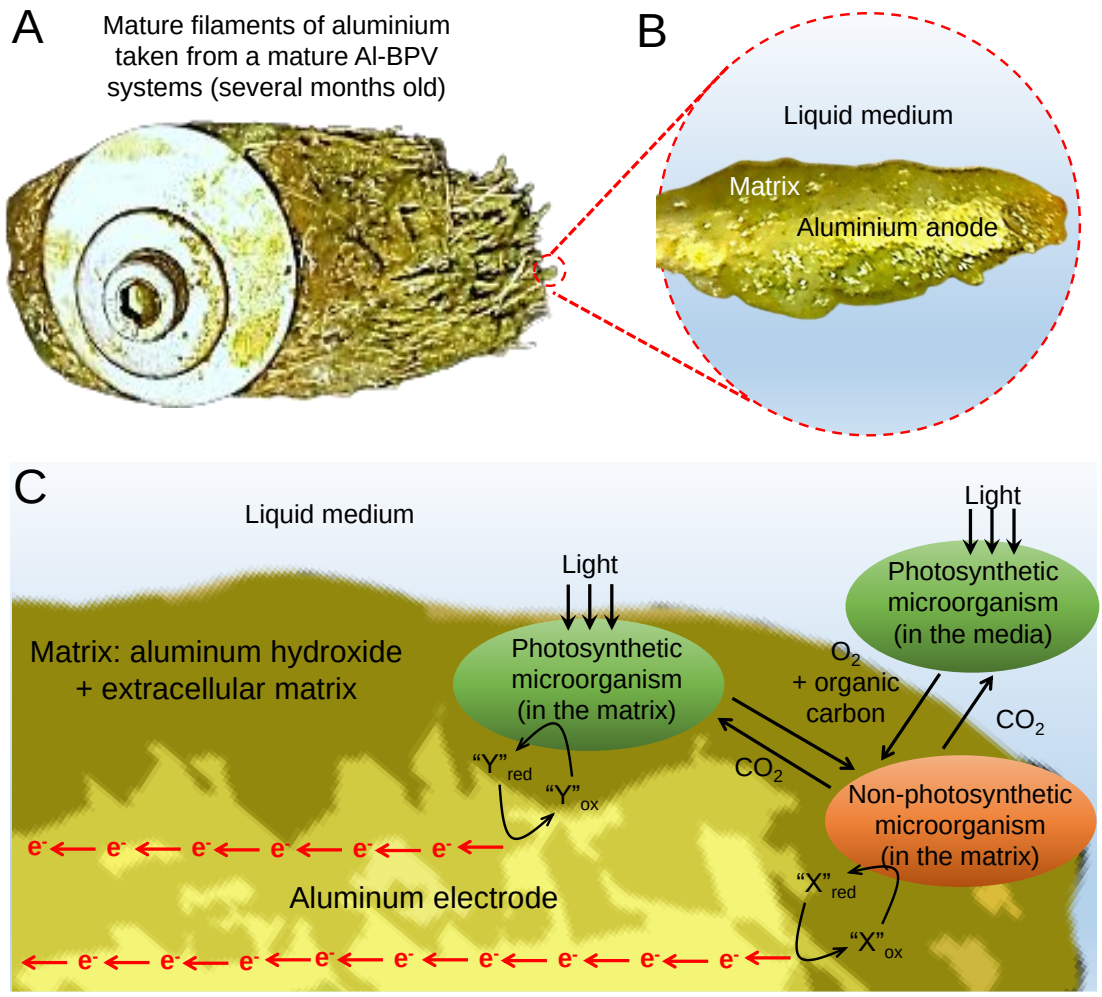

Fig.S16. Mechanism of electron transport. **A**) The aluminium anode taken from a mature Al-BPV system. **B**) Magnification of a filament of the aluminium anode taken from a mature Al-BPV system with the position of the actual anode and the matrix (aluminium hydroxide and extracellular components) annotated. **C**) Proposed mechanisms of electron transport within the mix of aluminium hydroxide and extracellular matrix.

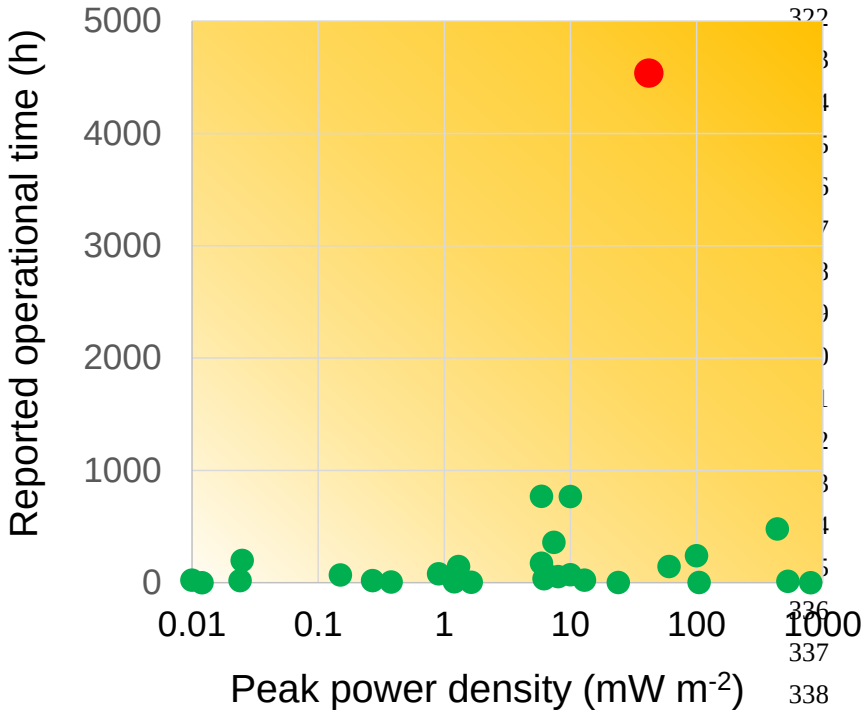

Fig. S17. The performance of our Al-BPV system (red marker) in terms of operational time *versus* peak power density, compared with the published state of the art of this technology. The data are given in **ST1**.

Table S1. List of publications consulted to generate **figure S17**. The operational time reported for the compact-Al-BPV in this present study was calculated based on the data presented in **figure 2**. Data not available are marked with n.a.

References	Ref	Peak power output ($mW\ m^{-2}$)	Max operational time (h)
Fu Chun-Chong, *et al*., *Bioresource Technology, 2009,* **100,** 4183–4186	1	1.64	5
Zou Yongjin, *et al*., *Biotechnology & Bioengineering*, 2009, **104**, 5	2	1.3	144
Fu Chun-Chong, *et al*., *Biochemical Engineering Journal, 2010,* **52**, 175–180	3	6.5	70
Pisciotta John M., *et al., PloS ONE*, 2010, **5**, 5, e10821	4	5.9	770
Zou Yongjin, *et al*., *Bioelectrochemistry*, 2010, **79**, 50–56	5	5.9	175
Bombelli P., *et al*., *Energy & Environmental Science*, 2011, **4,** 11, 4690-4698	6	1.2	8
McCormick A. J., *et al*., *Energy & Environmental Science*, 2011, **4**, 11, 4699-4709	7	10	768
Thorne R., *et al*., *J. Mater. Chem*., 2011, **21**, 18055	8	24	2
Bombelli P., *et al*., *PCCP*., 2012, **14**, 12221–12229	9	0.024	20
Madiraju K. S., *et al*., *Bioresource Technology*, 2012, **110**, 214–218	10	0.27	20
Raman K. *et al*., *Applied Energy*, 2012, **100**, 100–105	11	0.82	n.a.
Bradley R.W., *et al*., *PCCP*, 2013, **15,** 32, 13611-13618	12	0.181	n.a.
Chen W. J., *et al*., *ACS Appl. Mater. Interfaces*, 2013, **5**, 11123−11128	13	0.15	70
Inglesby A. E., *et al., PCCP*, 2013,**15**, 6903-691	14	0.025	200
Lan J.C.W., *et al*., *Biochemical Engineering Journal*, 2013, **78**, 39– 43	15	12.95	24
Lin C.C., *et al*., *Bioresource Technology*, 2013, **135**, 640–643	16	10	72
Luimstra V.M., *et al., J Appl Phycol*, 2014, **26**, 15–23	17	6.2	36
Schneider K., *et al*., *Philosophical Transactions A*, 2016, **374**, 20150080	18	7.4	360
Samsonoff N., *et al*., *Appl. Phys. Lett.*, 2014, **104**, 043704	19	0.012	1
Sekar N., *et al*., *Phys. Chem. Chem. Phys.*, 2014, **16**, 7862-7871	20	100	240
Ng F. L., *et al*., *PloS ONE*, 2014, **9**, 5, e97643	21	0.31	n.a.
Ng F. L., *et al*., *Scientific Report*, 2014, **4**, 7562	22	0.27	n.a
Bombelli P., *et al*., *Advanced energy materials*, 2015, **5**, 2, 1401299	23	105	2
Huang L.F., *et al*., *Int. J. Mol. Sci*., 2015, **16**, 19308-19325	24	0.01	24
S. Yoon et al., *NEMS***,** 2014**,** 391-398	25	0.9	80
Wei X., *et al*., *IEEE SENSORS*, 2016, *1-3*	26	60.5	144
Sawa M.**,** *et al*., Nature communications, 2017, **8**, 1, 1-10	27	0.38	7
Liu L. and Choi S., *Lab. Chip*, 2017, **17**, 3817–3825	28	438	480
Saar K. L. *et al*., *Nature energy*, 2018, **3,** 1, 75-81	29	530	12
Kim, M.J., *et al*., *Journal of Power Sources*, 2019, **412**, 301-310	30	806	1
This present study		42	4536

Materials and Methods

Synechocystis culture and growth

Wild-type *Synechocystis* sp. PCC6803 (hereafter *Synechocystis*) was routinely cultured in BG-11 medium[31] supplemented with 10 mM $NaHCO_3$ and maintained in sterile conditions at (30 ± 2) °C under continuous moderate light of 40 µmol photons m^{-2} s^{-1} and shaking at 160 revolutions per minute (rpm.). A bench-top centrifuge (5,000 rpm for 3 min) was used to concentrate the cells. The concentration of chlorophyll in samples was determined spectrophotometrically from the optical density values at 680 nm and 750 nm as described previously[32] (Lea-Smith *et al.*, 2013).

Growth Assays in the Presence of Aluminium

To perform growth assays in the presence of aluminium (**Fig.S1**), cultures were prepared by inoculating 3 independent colonies growing on an agar plate into 20 mL of BG11 medium[31] in 50 mL Nunc™ flasks. Cultures were grown photoautotrophically in an Infors incubator at 30 °C under 40 µE m^{-2} s^{-1} continuous white fluorescence light, shaking at 120 rpm. After 5 days, 5 mL from each culture was diluted in 35 mL of BG11 in three new Nunc flasks, resulting in three replicates (each containing an initial OD_{750} ≅ 0.25) for growth without aluminium. To quantify growth in the presence of aluminium, 1.5 grams of fine-grade aluminium wool (Rogue River Tools, USA) (**Fig.S2**) were weighed and inserted at the bottom of three additional flasks. These flasks were then filled with 5 mL of precultures and 35 mL of sterile BG11 medium. Before inserting the aluminium wool in the sterile flasks, aluminium filaments were cleaned according to a protocol described by Kumari *et al.* (2019)[33]. Briefly, dirt was removed by etching electrodes in a 7.5 wt% solution of NaOH, then the electrodes were cleaned in concentrated HNO_3, thoroughly rinsed in deionised water and then autoclaved. The 6 flasks were then grown for six days under photoautotrophic conditions in an Infors incubator at 30 °C under 40 µE m^{-2} s^{-1} continuous white light, shaking at 120 rpm. Every other day, optical density measurements were performed using a Shimadzu UV-1800 (Shimadzu, United Kingdom) spectrophotometer, recording absorbance spectra between 400-750 nm, using BG11 and BG11 + aluminium wool as blanks.

Colonising the aluminium anode with *Synechocystis*

Electrochemical characterisation of *Synechocystis* biofilms was performed on previously colonised aluminium electrodes transferred into single-chamber, two-electrode biophotovoltaic

devices. To colonise the aluminium wool electrodes, a ~29L photobioreactor was constructed using transparent fish tanks (40 x 25.5 x 28cm) as reactor vessels. Each tank contained 18 aluminium anodes stacked in parallel using a stainless steel bar and was filled with 20 L of sterile BG11 medium. Each aluminium anode was assembled with 1.5 grams of 10 cm long fine-grade aluminium wool (Rogue River Tools, USA) (**Fig.S2**). The aluminium threads were held together by marine-grade stainless-steel washers and bolts. Each tank was bubbled with filtered air pumped using air pumps and plastic tubing and was stirred with magnetic stirrer bars. Each tank was illuminated from the top by two 9W LED bars (RS components, United Kingdom). Before inoculating the reactor with cells, the tanks were sterilised with 70% ethanol and UV radiation. The aluminium electrodes were cleaned according to the protocol described above (Kumari et al. 2019). After two weeks of operation at room temperature at 12 hours light /6 hours dark cycles, individual electrodes from the reactor vessel were transferred into prototype Al-BPV electrochemical cells.

Developing the prototype Al-BPV

The prototype Al-BPV were assembled as follows. The aluminium anodes were formed as previously described and transferred into a single-chamber prototype. The chamber was made with a Perspex tube of 40 mm external diameter, 36 mm internal diameter and 200 mm long. Each aluminium anode was assembled with 1.5 grams of 10 cm long fine-grade aluminium wool (Rogue River Tools, USA) (**Fig.S2**). The aluminium threads were held together and secured to the Perspex tube by marine-grade stainless-steel washers and bolts (RS Components, UK). The cathode consisted of coated carbon paper/Pt (loading 3 mg cm^{-2}, Alfa Aesar 45372 Hydrogen Electrode/Reformate, USA). The cathode was secured at one end of the Perspex tube with a McAlpine T28M Straight Connector 40mm x 40mm (ScrewFix, UK), a rubber O-ring and a 36mm diameter stainless-steel washers (RS Components, UK) to ensure a secure connection (**Fig.S3** and **Fig.S4A**). The prototype Al-BPV were filled with ~200 mL of sterile BG11 medium.

Electrochemical characterisation of prototype Al-BPV in laboratory-controlled environment

The electrical output of the prototype Al-BPVs containing individual aluminium electrodes was measured and recorded with a multi-channel MultiEmStat3 Potentiostat (PalmSense, UK) in chronoamperometry mode at applied bias potential of 0 V. Recordings were taken every 5 seconds

for ~36 hours (**Fig.S4B**). Experiments were conducted at 12 hours cycle (6 hour light / 6 hour dark), illuminated from the top by a 3W warm-white LED (RS components, UK). The experimental run was conducted in a laboratory-controlled environment at 22 ± 2 °C throughout the characterization process. Experiments were repeated at least three times with three independently colonised electrodes.

After chronoamperometric measurements, linear sweep voltammetry from -0.8V to 0V was performed at scan rate of 0.0001 V/s both in dark and light conditions, illuminated from the top by a 3W LED (RS components, United Kingdom) to derive the peak power and maximum current as shown in the power curved (**Fig.S4C**). The experimental run was conducted in a laboratory-controlled environment at 22 ± 2 °C throughout the characterization process.

Effect of DCMU on the photo-current

For photocurrent inhibition experiments (**Fig.1B**), 30 µL of 3-(3,4-dichlorophenyl)-1,1-dimethylurea (DCMU, CAS number: 330-54-1; Sigma, UK) from a 0.1 M stock (final concentration = 15 µM) was added into the anodic chamber of the BPV whilst current output was measured and recorded with a multi-channel MultiEmStat3 Potentiostat (PalmSense, UK) in chronoamperometry mode at applied bias potential of 0 V. Experiments were conducted with a 4 hours cycle (2 hour light / 2 hour dark), illuminated from the top by a 3W LED (RS components, UK). The experimental run was conducted in a laboratory-controlled environment at 22 ± 2 °C throughout the characterization process (**Fig.1B**)

Autofluorescence and current output

Autofluorescence was observed from a prototype Al-BPV system equipped with an aluminium anode colonised with photosynthetic microorganisms several months old. The experiment was conducted using a setup (**Fig.S5A**) including a custom-made light emission device fitted with a LZC-00MC40 RGB LED light (RS Components, UK). Blue light (350 µE m^{-2} s^{-1}, peak emission at λ=475nm) was shone from the top into the anodic chamber of the Al-BPV system through the transparent Perspex. The LED light spectra (**Fig.S5B**, blue line) was measured using a Spectrometer USB2000+UV-VIS detector (Ocean Optics, US). A digital camera was placed behind an optical filter and focused on the aluminium filaments of the colonised anode. The transmission spectrum of the optical filter peaked at λ=688nm (**Fig.S5B**, red line).

Autofluorescence was observed whilst current output was measured in chronovoltammetry mode with an external load of 10 kΩ (**Fig.S5C** black line) using a multi-channel MultiEmStat3 Potentiostat (PalmSense, UK) as previously described. To enhance the autofluorescence 10 frames were digitally combined to form the image shown in **Figure S5D**.

The aluminium anode colonised with photosynthetic microorganisms was removed from the anodic chamber of the Al-BPV system and autoclaved (20 min, 121 °C, 15 psi). The autoclaved electrode was reinstalled in the anodic chamber of the Al-BPV system and used to re-assess the current output (**Fig.S5C** blue line) and autofluorescence (**Fig. S5E**) measured as for the aluminium electrode before autoclaving.

Developing a compact Al-BPV

The body of the compact Al-BPV was made by a block of acrylic (Engineering & Design Plastics Ltd, UK) 60mm hight and 31 x 23 mm wight in total. The block has three internal voids as displayed in **Figure S6**. The total external volume of the acrylic body was 44.8 mL with an internal operative volume of 14.4 mL. Two stainless-steel (S/S) plates (75 mm x 25 mm x 2.5 mm, RS Components, UK) are secured on the front and back of the acrylic body using 10 M5 stainless-steel screws (RS Component, UK). On one side (cathodic side), the stainless-steel plate was used to hold in place a thin film of polytetrafluoroethylene (PTFE, Hansatech Instruments Ltd., UK) and a carbon paper/Pt cathode (~2.5 cm^2, loading 3 mg cm^{-2}, Alfa Aesar 45372 Hydrogen Electrode/Reformate, USA). On the other side (anodic side), the stainless-steel plate was used to hold in place another thin film of polytetrafluoroethylene (PTFE, Hansatech Instruments Ltd., UK) and provide a docking area in which to fasten the aluminium anode by using an M5 stainless-steel screws and washers (RS Component, UK). The aluminium anode was made of 0.7 grams of fine-grade aluminium wool (Rogue River Tools, USA). The aluminium electrodes were cleaned according to the protocol described above[33]. The complete compact Al-BPV system is shown in **Figure S7**.

Electrochemical characterisation of compact Al-BPV in laboratory-controlled environment

The electrical output of the prototype Al-BPVs containing individual aluminium electrodes was measured and recorded with a multi-channel MultiEmStat3 Potentiostat (PalmSense, United Kingdom). The compact Al-BPV system constructed as described above was injected with

Synechocystis (36.5 nmol Chl) suspended in BG11 medium.

Linear sweep voltammetry from -1V to 0V was performed at a scan rate of 0.0001 V/s both in dark and light conditions (illuminated from the side, ~500 µE m^{-2} s^{-1} by a 3W LED, RS components, United Kingdom) to derive the peak power and maximum current as shown in the power curves (**Fig.1E**). The experimental run was conducted in a laboratory-controlled environment at 22 ± 2 °C throughout the characterization process.

After the linear sweep voltammetry measurements, the compact Al-BPV was tested in chronovoltammetry mode with an external load of 10 kΩ (two electrode system) for about 23 days at 2 hours cycle (1 hour light / 1 hour dark), illuminated from the side ~500 µE m^{-2} s^{-1} by a 3W LED (RS components, UK) (**Fig.S8**).

Testing the compact Al-BPV for powering the Arm Cortex-M0+ Processor in a domestic environment

After having characterised the compact Al-BPV system in controlled laboratory conditions, the device was connected using crocodile clips to the negative and positive terminals of the test-chip with the Cortex-M0+ microprocessor. The test-chip contained a LED to indicate whether sufficient power was being drawn from the compact Al-BPV device to sustain the microprocessor's operation. After observing that the LED was illuminated, the device was then left in the vicinity of a window in a domestic environment (Cambridge, UK, **Fig.S10**). The test-chip board verifies the operation of the processor and measures the potential and intensity of the electrical output of the compact Al-BPV system. Data were transferred to the Internet-cloud via a Raspberry-pi/router and the ThingSpeak™ platform was used to record and visualise the data (**Fig.S11**).

CPU operation (computing mode and standby mode)

The CPU was programmed to perform 45 minutes of computation work (computing Gaussian sum with a frequency of 10 kHz) followed by 15 minutes in stand-by mode (no computation). The experiment shown in **Figure 2** was entirely run following this alternating mode (computation / standby). By contrast, the experiment shown in **Figure S12** included a first phase (week 0 to week 13) of continuous computation followed by a second phase (week 15 to week 20) of alternating mode (computation / standby).

Domestic environment and experimental setup where the compact Al-BPV was used to power the CPU

The compact Al-BPV was placed at the window sill in a living room of a domestic property located in Cambridge (UK), latitude: 52.23 / 52°14'0"N; longitude: 0.1329 / 0°7'58"E (**Fig.S10**). The compact Al-BPV was exposed to ambient lighting as recorded by a light probe mounted on the test-chip (**Fig.2J-L**). To compensate for water evaporation through the teflon membranes (Callapg, https://www.goodyearrubberproducts.com/2012pdfs/O_rings_Catalog/files/assets/downloads/page0009.pdf, accessed on 13/12/2021), two to three mL of commercial still drinking water (Still Spring Water, Harrogate, UK) was added every 7-10 days, depending on the rate of evaporation due to variation in ambient temperature.

CPU induced failure

To test system failure a drop in temperature was forced by positioning an ice-pack near the temperature probe mounted on the test-chip, causing a localised lowering of ambient temperature below 5 °C, and automatically switching the powering of the CPU from the Al-BPV to the mains electricity (USB powered), recording a voltage of >5V. To revert the powering of the CPU from the mains electricity (USB powered) to the Al-BPV, the system would need to be reset manually.

Optical microscopy investigations

Optical microscopy images were taken with a RS PRO, 10 – 100X, ris. 2M pixel, digital optical microscope USB-interfaced (RS Component, UK).

SEM – scanning electro microscopy investigations

Scanning electron microscopy of bare Al filaments and filaments from AL-BPV was performed using a Supra 55-VP SEM (Zeiss) in SE2-mode with a 2kV accelaration voltage. As only coverage was to be investigated, no biological fixation step was conducted.

CVs performed on a mix of aluminium hydroxide and extracellular matrix scraped from the anode of a mature Al-BPV system

Cyclic voltammetry measurements were carried out with a multi-channel MultiEmStat3 Potentiostat (PalmSense, UK). Small samples of the biofilm and extracellular matrix were scraped

from the colonised aluminium anode several months old and placed on the working electrode of a Screen-Printed Gold Electrode C223BT (Aux.:Au; Ref.:Ag) / Ink BT. Working Electrode of 1.6 mm diameter (Metrohm, UK). A drop (200 µL) of fresh BG11 was placed above the scraped material on the printed electrodes. After 6 hours of resting, cyclic voltammetry measurements (21 scans) were carried out at 5 mV s^{-1} between −800 mV and 800 mV.

Impedance electrochemical spectroscopy (EIS) and potentiodynamic sweep (PDS) measurements

All electrochemical measurements were performed in growth medium in a three-electrode cell. The working electrode was bare Al filaments or filaments from a compact Al-BPV after ca. four months of operation. The counter electrode was a platinum plate with a surface area considerably larger than that of the working electrode, and the reference electrode used saturated Ag/AgCl. Electrochemical impedance measurements (EIS) and potentiodynamic sweeps (PDS) were performed in BG11 in a three-electrode cell. To ensure there was no biological activity the filaments from the Al-BPV were immersed in absolute alcohol for 30 minutes prior to testing. EIS and PDS were carried out after 60 min of open-circuit potential measurements. The EIS measurements were carried out over a frequency range from 100 kHz to 10 mHz using a 10 mV amplitude of sinusoidal variation around the E_{ocp}. The PDS measurements were carried out from a cathodic negative potential of −0.250 V to a positive anodic potential of 1.5 V with respect to initial E_{ocp}, at a scan rate of 0.168 mV/s. All measurements were recorded using an Iviumstat.Xre potentiostat connected to an Ivium Boost current enhancer.

Microbiome analysis

Biological material in the supernatant fraction of samples was harvested by centrifugation (14,000 x g for 5 min) and the supernatant discarded. The anode matrix sample was gently inverted to allow loosely associated biofilms to be dislodged from the aluminium wool anode. The suspended material was transferred to a sterile centrifuge tube and large particulates settled-out for 10 min. prior to removal of the overlying supernatant fraction. The supernatant cell pellets, particulates and aluminium wool were individually snap-frozen in liquid nitrogen and stored at -80˚C prior to DNA extraction. Total DNA was extracted by pre-treating samples with lysozyme (250 µg in 50 µl of 10 mM Tris-HCl pH 8.0 and 1 mM EDTA for 30 min. at 37˚C), then the DNeasy Plant Mini

kit (Qiagen) was used as recommended by the manufacturer.

Paired-end amplicon sequencing (PE250) of 16S rRNA genes was performed using the V3-V4 universal bacterial primers 341F (5'-CCTAYGGGRBGCASCAG -3') and 806R (5'-GGACTACNNGGGTATCTAAT -3') using Illumina HiSeq platform (Novogene UK, Ltd). Paired-end reads were split according to their unique barcodes and primers and barcodes truncated. Subsequently, particulate and aluminium wool fastq paired-reads were concatenated to create a single 'matrix' paired-read sample. DADA2[34] was used to quality filter, dereplicate and de-noise truncated reads prior to chimera removal. Taxonomic inference of the 'liquid media' and 'matrix' samples was based on the DADA2 implementation of the Naïve Bayesian classifier[35] trained using SILVA 138 database release[36]. Microbial community analysis of amplicon sequence variants was performed using routines in *phyloseq* version 1.34.0[37] in R vers. 4.0.3[38]. The data for this study have been deposited in the European Nucleotide Archive (ENA) at EMBL-EBI under accession number PRJEB46799 (https://www.ebi.ac.uk/ena/browser/view/PRJEB46799).

Data availability

The data that support the plots within this paper and other findings of this study are available at: https://doi.org/10.17863/CAM.74822

Supplementary References

[1] C.C. Fu, C.H. Su, T.C. Hung, C.H. Hsieh, D. Suryani and W.T. Wu, Effects of biomass weight and light intensity on the performance of photosynthetic microbial fuel cells with Spirulina platensis. *Bioresource Technology*, 2009, **100**, 4183–4186.

[2] Y. Zou, J. Pisciotta, R.B. Billmyre and I.V. Baskakov, Photosynthetic microbial fuel cells With positive light response, *Biotechnology and Bioengineering*, 2009, **104**, 5, 930-946.

[3] C.C. Fu, T.C. Hung, W.T. Wu, T.C. Wen and C.H. Su, Current and voltage responses in instant photosynthetic microbial cells with Spirulina platensis. *Biochemical Engineering Journal*, 2010, **52**, 175–180.

[4] J.M. Pisciotta, Y. Zou and I.V. Baskakov, Light-dependent electrogenic activity of cyanobacteria, *PloS ONE*, 2010, **5**, e10821.

[5] Y. Zou, J. Pisciotta and I.V. Baskakov, Nanostructured polypyrrole-coated anode for sun-powered microbial fuel cells. *Bioelectrochemistry*, 2010, **79**, 50–56.

[6] P. Bombelli, R.W. Bradley, A.M. Scott, A.J. Philips, A.J. McCormick, S.M. Cruz, A. Anderson, K. Yunus, D.S. Bendall, P.J. Cameron, J.M. Davies, A.G. Smith, C.J. Howe and A.C. Fisher, Quantitative analysis of the factors limiting solar power transduction by Synechocystis sp. PCC 6803 in biological photovoltaic devices, *Energy & Environmental Science* 4, 2011, **11**, 4690-4698.

[7] A.J. McCormick, P. Bombelli, A.M. Scott, A.J. Philips, A.G. Smith, A.C. Fisher and C.J. Howe, Photosynthetic biofilms in pure culture harness solar energy in a mediatorless bio-photovoltaic cell (BPV) system, *Energy & Environmental Science*, 2011, **4,** 11, 4699-4709.

[8] R. Thorne, H. Hu, K. Schneider, P. Bombelli, A. Fisher, L.M. Peter, A. Dent and P.J. Cameron, Porous ceramic anode materials for photo-microbial fuel cells, *J. Mater. Chem.*, 2011, **21**, 18055.

[9] P. Bombelli, M. Zarrouati, R.J. Thorne, K. Schneider, S.J. Rowden, A. Ali, K. Yunus, P.J. Cameron, A.C. Fisher, D. Ian Wilson, C.J. Howe and A.J. McCormick, Surface morphology and surface energy of anode materials influence power outputs in a multi-channel mediatorless bio-photovoltaic (BPV) system, *Phys. Chem. Chem. Phys.*, 2012, **14**, 12221–12229.

[10] K.S. Madiraju, D. Lyew, R. Kok and V. Raghavan, Carbon neutral electricity production by Synechocystis sp. PCC6803 in a microbial fuel cell, *Bioresource Technology*, 2012, **110**, 214–218.

[11] K. Raman and J.C.W. Lan, Performance and kinetic study of photo microbial fuel cells (PMFCs) with different electrode distances, *Applied Energy*, 2012, **100**, 100–105.

[12] R.W. Bradley, P. Bombelli, D.J. Lea-Smith and C.J. Howe, Terminal oxidase mutants of the cyanobacterium Synechocystis sp. PCC 6803 show increased electrogenic activity in biological photo-voltaic systems, *Phys. Chem. Chem. Phys.*, 2013, **15**, 13611-13618.

[13] W. Chen, M. Lee, J.L. Thomas, P. Lu, M. Li and H. Lin, Microcontact Imprinting of Algae on Poly(ethylene-co-vinyl alcohol) for Biofuel Cells, *ACS Appl. Mater. Interfaces*, 2013, **5,** 11123−11128.

[14] A.E. Inglesby, K. Yunus and A.C. Fisher, In situ fluorescence and electrochemical monitoring of a photosynthetic microbial fuel cell. *Phys. Chem. Chem. Phys.*, 2013,**15**, 6903-691.

[15] J.C.W. Lan, K. Raman, C.M. Huang and C.M. Chang, The impact of monochromatic blue

and red LED light upon performance of photo microbial fuel cells (PMFCs) using *Chlamydomonas reinhardtii* transformation F5 as biocatalyst. *Biochemical Engineering Journal*, 2013, **78**, 39– 43.

[16] C.C. Lin, C.H. Wei, C.I. Chen, C.J. Shieh and Y.C. Liu, Characteristics of the photosynthesis microbial fuel cell with a *Spirulina platensis* biofilm. *Bioresource Technology*, 2013, **135**, 640–643.

[17] V.M. Luimstra, S.J. Kennedy, J. Güttler, S.A. Wood, D.E. Williams and M.A. Packer, A cost-effective microbial fuel cell to detect and select for photosynthetic electrogenic activity in algae and cyanobacteria, *J. Appl. Phycol.*, 2014, **26**, 15–23.

[18 K. Schneider, R.J. Thorne and P.J. Cameron, An investigation of anode and cathode materials in photomicrobial fuel cells, *Philosophical Transactions A*, 2016, **374**, 20150080.

[19] N. Samsonoff, M.D. Ooms and David Sinton, A photosynthetic-plasmonic-voltaic cell: Excitation of photosynthetic bacteria and current collection through a plasmonic substrate, *Appl. Phys. Lett.*, 2014, **104**, 043704.

[20] N. Sekar, Y. Umasankar and R.P. Ramasamy, Photocurrent generation by immobilized cyanobacteria via direct electron transport in photo-bioelectrochemical cells, *Phys. Chem. Chem. Phys.*, 2014, **16**, 7862-7871.

[21] F.L. Ng, S.M. Phang, V. Periasamy, K. Yunus, A.C. Fisher, Evaluation of algal biofilms on Indium Tin Oxide (ITO) for use in biophotovoltaic platforms based on photosynthetic performance, *PloS ONE*, 2014, **9**, e97643.

[22] F.L. Ng, M.M. Jaafar, S.M. Phang, Z. Chan, N.A. Salleh, S.Z. Azmi, K. Yunus, A.C. Fisher and V. Periasamy, Reduced graphene oxide anodes for potential application in algae biophotovoltaic platforms, *Sci. Rep.*, 2014, **4**, 7562.

[23] P. Bombelli, T. Müller, T.W. Herling, C.J. Howe and T.P.J. Knowles, A high power-density, mediator-free, microfluidic biophotovoltaic device for cyanobacterial Cells, *Advanced Energy materials*, 2015, **5**, 1401299.

[24] L.F. Huang, J.Y. Lin, K.Y. Pan, C.K. Huang and Y.K. Chu, Overexpressing ferredoxins in Chlamydomonas reinhardtii increase starch and oil yields and enhance electric power production in a photo microbial fuel cell. *Int. J. Mol. Sci.*, 2015, **16**, 19308-19325.

[25] S. Yoon, H. Lee, A. Fraiwan, C. Dai and S. Choi, A micro-sized microbial solar cell. *The 9th IEEE International Conference on Nano/Micro Engineered and Molecular Systems (NEMS)*,

2014, 265-268.

[26] X. Wei, M. Mohammadifar, W. Yang and S. Choi, A Microscale Biophotovoltaic Device**,** *2016 IEEE SENSORS, 2016,* 1-3.

[27] M. Sawa, A. Fantuzzi, P. Bombelli, C.J. Howe, K. Hellgardt and P.J. Nixon, Electricity generation from digitally printed cyanobacteria, *Nature Communications,* 2017, **8**, 1, 1-10.

[28] L. Liu and S. Choi. Self-sustainable, high-power-density bio-solar cells for lab-on-a-chip applications, *Lab. Chip*, 2017, **17**, 3817–3825.

[29] K.L. Saar, P. Bombelli, D.J. Lea-Smith, T. Call, E.M. Aro, T. Müller and C.J. Howe and T.P.J. Knowles, Enhancing power density of biophotovoltaics by decoupling storage and power delivery, *Nature Energy*, 2018, **3**, 75-81.

[30] M.J. Kim, S.J. Bai, J.R. Youn, Y.S. Song. Anomalous performance enhancement effects in Ruthenium-based Dye Sensitized Solar Cells. *Journal of Power Sources*, 2019, **412**, 301-310.

[31] R. Rippka, R.Y. Stanier, J. Deruelles, M. Herdman and J.B. Waterbury, Generic assignments, strain histories and properties of pure cultures of cyanobacteria. *Journal of General Microbiology*, 1979, **111**, 1-61.

[32] D.J. Lea-Smith, N. Ross, M. Zori, D.S. Bendall, J.S. Dennis, S.A. Scott, A.G. Smith and C.J. Howe, Thylakoid terminal oxidases are essential for the cyanobacterium *Synechocystis* sp.PCC 6803 to survive rapidly changing light intensities. *Plant. Physiol.*, 2013, **162**, 484–495.

[33] S. Kumari, S. Wenner, J.C. Walmsley, O. Lunder and K. Nisancioglu, Progress in understanding initiation of intergranular corrosion on AA6005 aluminum alloy with low copper content, *Journal of The Electrochemical Society*, 2019, **166**, C3114–C3123.

[34] B.J. Callahan, P.J. McMurdie, M.J. Rosen, A.W. Han, A.J.A. Johnson and S.P. Holmes, DADA2: High-resolution sample inference from Illumina amplicon data, *Nat. Methods*, 2016, **13**, 7, 581-583.

[35] Q. Wang, G.M. Garrity, J.M. Tiedje and J.R. Cole, Naive Bayesian classifier for rapid assignment of rRNA sequences into the new bacterial taxonomy, *Appl. Environ. Microbiol.*, 2007, **73**, 5261-5267.

[36] P. Yilmaz, L. Wegener Parfrey, P. Yarza, J. Gerken, E. Pruesse, C. Quast, T. Schweer, J. Peplies, W. Ludwig and F.O. Glöckner, The SILVA and All-species Living Tree Project (LTP)

taxonomic frameworks, *Nucleic Acids Res.*, 2014, **42**, D643-648.

[37] P.J. McMurdie and S. Holmes, Phyloseq: an R package for reproducible interactive analysis and graphics of microbiome census data, *PLoS One*, 2013, **8**, e61217.

[38] R Core Team (2018). R: A language and environment for statistical computing. R Foundation for Statistical Computing, Vienna, Austria. Available online at https://www.R-project.org/.